EPJ Nuclear Sci. Technol. **6**, 47 (2020)

https://doi.org/10.1051/epjn/2020008

EPJ Nuclear Sciences & Technologies

Available online at:
https://www.epj-n.org

REGULAR ARTICLE

OPEN ACCESS

An improved method to evaluate the "Joint Oxyde-Gaine" formation in (U,Pu)O_2 irradiated fuels using the GERMINAL V2 code coupled to Calphad thermodynamic computations

Karl Samuelsson[1,*], Jean-Christophe Dumas[2,**], Bo Sundman[3], and Marc Lainet[2]

[1] KTH Royal Institute of Technology, Nuclear Engineering, 106 91 Stockholm, Sweden
[2] CEA, DEN, DEC, Centre de Cadarache, 13108, Saint-Paul-lez-Durance, France
[3] OpenCalphad, 9 Allée de l'Acerma, 91190 Gif-sur-Yvette, France

Received: 20 September 2019 / Received in final form: 2 December 2019 / Accepted: 21 February 2020

Abstract. In this work, two different thermodynamic softwares, ANGE using the TBASE database, and OpenCalphad using the TAF-ID (Thermodynamics of Advanced Fuels – International Database), have been integrated into the GERMINAL V2 fuel performance code (of the PLEIADES platform) in order to evaluate the chemical state of (U,Pu)O_2 fuel and fission products in sodium cooled fast reactors. A model to calculate the composition and the thickness of the "Joint-Oxyde Gaine" (JOG) fission product layer in the fuel-clad gap has been developed. Five fuel pins with a final burnup ranging between 3.8 and 13.4% FIMA (Fissions per Initial Metal Atom) have been simulated, and the calculated width of the fission product layer have been compared with post irradiation examinations. The two different thermodynamic softwares have been compared in terms of computation time and predicted fuel-to-clad gap chemistry. The main elements and phases encountered in the fission productlayer have been identified, and the impact of the changing oxygen potential has been explored.

1 Introduction

When oxide fuel pins are irradiated in a fast breeder reactor (FBR), it has been observed that certain fission products (FP) migrate down the temperature gradient and form a layer between the fuel and the stainless steel cladding. This layer of fission product compounds is commonly called JOG (for "Joint Oxyde-Gaine" in French) [1], and the fact that its presence affects both heat transfer and corrosion rates [2,3] has warranted attempts to understand and predict its formation. Internal corrosion weakens the cladding and increases the probability of fuel failure, especially at high burnup [4]. As described in reference [1], JOG was first proposed as an explanation for an inconsistency found in these PIE: if the large fuel-to-clad gap that appears at high burnup had only been filled with gas, it would certainly have caused fuel melting (due to the poor heat conductivity of the gas). However, if the gap was to be partly filled with fission product compounds with higher thermal conductivity compared with the gas plenum, the maximum fuel temperature would fall below the melting point of the fuel. These FP would need to be transported through the fuel towards the periphery due to the effect of the thermal gradient. This could later be confirmed by experimental observations and measurements. Inoue et al. [2] concludes, after studying irradiated MOX fuel pins in the fast neutron JOYO reactor, that JOG evolution is dependent on burnup, temperature, initial fuel microstructure, and fission gas release. These variables are of course not independent of one another. The exact composition of this JOG layer has never been determined, and the term itself can be seen as an umbrella term for any FP that has deposited in the fuel-to-clad gap. While it is believed to be rich in Mo and Cs oxides, the distribution of phases is likely heterogeneous [5].

The GERMINAL V2 [6] fuel performance code, developed by the CEA (French Alternative Energies and Atomic Energy Commission) within the PLEIADES simulation platform [7], is used to simulate the thermo-mechanical and the physico-chemical behavior of (U,Pu)O_2 fuel during irradiation in a fast neutron spectrum. In its current version, the prediction of JOG thickness is described by a model involving the amount of volatile FP (mainly caesium) based on a correlation to the kinetics of the release of the stable fission gases [6,8]. A threshold in burnup as well as a thermal activation term are respectively

* e-mail: karlsam@kth.se
** e-mail: jean-christophe.dumas@cea.fr

Table 1. Data for the simulated fuel pins. Predicted FGR fraction refers to the value predicted by Germinal V2. Both this parameter and burnup are taken at the peak power node.

Name of Phénix experiment	Maximum burnup [%FIMA]	Predicted FGR fraction	Initial ratio O/M	Pu/M
Hadix-1	3.8	0.60	1.986	0.1979
Boitix-1	7.0	0.75	1.978	0.1945
Coucou-1	9.0	0.71	1.987	0.2022
Sphinx-1	11.2	0.82	1.983	0.2068
Nestor-3	13.4	0.90	1.975	0.2246

O-Oxygen, Pu-Plutonium, M-Metal, FGR-Fission Gas Release

used to reproduce the post-irradiation observations showing no JOG formation at low burn-up and at low linear power.

In the past years, several groups have worked on implementing thermodynamic calculations inside fuel performance codes in order to improve predictive abilities. Baurens et al. [9] and later Konarski et al. [10] have coupled Ange together with the Alcyone (also in the Pleiades simulation platform) in order to simulate, respectively, stress corrosion cracking and oxygen thermodiffusion. Simunovic et al. [11] have coupled Thermochimica [12] to the mass and heat transport models of the Bison [13] fuel performance code. Both these examples have been focusing on the simulation of light water reactor fuel. Uwaba et al. [14] at the Japan Atomic Energy Agency have recently coupled the Mlcyone [15,16] caesium behavior simulation code to the Cedar [17] fast reactor fuel performance code. This has allowed for predictions on the JOG chemistry and geometry.

In this work, two different thermodynamic softwares, both based on the Calphad method [18,19], have been integrated into Germinal V2 in order to calculate the chemical state of the fuel. Full in-pile simulations have been performed on five fuel pins with different burnup ranging between 3.8 and 13.4 %FIMA burnup. JOG thickness has then been estimated on the basis of the predicted chemical composition of the gap and the known molar volumes of the involved phases. The two different thermodynamic solvers, Ange [20] and OpenCalphad [21,22], and their respective databases have been compared in terms time and prediction of JOG thickness and its composition. When available, results have been compared with experimental results. In a separate set of stand-alone calculations, the thermodynamic codes have also been evaluated and compared in terms of computational cost.

2 Experiments

The operation of the Phénix reactor between 1973 and 2010 associated with numerous post irradiation examinations (PIE) by the CEA resulted in an extensive database of fuel pin behavior under irradiation in a fast neutron spectrum.

In this work, five fuel pins from the Phénix fast breeder reactor irradiated to different burnup (3.8, 7.0, 9.0, 11.2, and 13.4 %FIMA at the maximum flux plane) have been simulated with Germinal V2. More information concerning the fuel pins can be found in Table 1. Previous PIE have given experimental values for measured JOG thickness of fuel pins irradiated in the Phénix reactor, see Figure 1. It should be noted that these experimental values are measurements of the fuel-to-clad gap, and are only *assumed* to be equal to JOG thickness for reasons mentioned above. The fuel pins were generating between 350 and 400 W/cm and the highest temperatures reached at the peak power nodes were, depending on the fuel pin between 2200 and 2400 K (based on the Germinal V2 simulations).

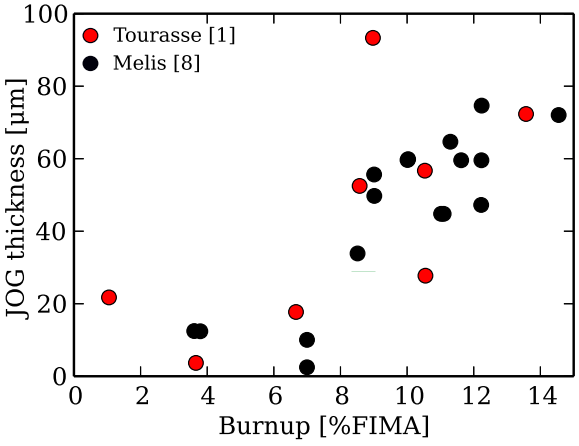

Fig. 1. Measured JOG thickness versus final burnup in some SFR fuel pins irradiated in the Phénix reactor. For reference [1], the burnup values refer to the local burnup at which the JOG was measured. For reference [8], the burnup refers to the maximum burnup reached in the fuel pin.

3 Method

3.1 Thermodynamic software and databases

For the calculations, two different software-database combinations have been used and compared:

– Ange (Advanced Numeric Gibbs Energy minimizer) [20], co-developed by CEA and EDF (Electricité de France), based on the Solgasmix [23–25] software.

– OpenCalphad open source software [21,22] using the TAF-ID [26,27] database which is the result of the merging of several databases (including TBASE).

The main advantage of OpenCalphad is its ability to utilize better thermodynamic models in the newer (and still growing) TAF-ID database, but comes at the price of increased computational time as will be discussed in Section 3.2. The purpose of the TAF-ID project, coordinated by the Organization for Economic Co-operative Development Nuclear Energy Agency (OECD/NEA), is to provide a comprehensive thermodynamic database on nuclear fuel materials to perform a wide range of thermodynamic calculations for different applications of nuclear reactors. This database can be seen as a synthesis of different databases (including TBASE) developed independently in different countries and has been progressively extended for five years by introducing either models coming from research and/or databases of the participants of the project, or coming from the open literature. It has been decided to adopt a full Calphad modeling approach for this database in order to provide both phase diagram and thermodynamic data calculations. Here, the description of the $(U,Pu,Ln)O_{2\pm x}$ phase is based on the Compound Energy Formalism (CEF) [28] model of Guéneau et al. [29]. This phase, made up by three sublattices, can be written as $(Ba^{2+}, Ce^{3+}, Ce^{4+}, Gd^{3+}, La^{3+}, Pu^{3+}, Pu^{4+}, U^{3+}, U^{4+}, U^{5+}, Zr^{2+}, Zr^{4+})_1 (O^{2-},Va)_2(O^{2-},Va)_1$ where Va indicates a vacancy.

For the liquid phases, the two sublattice ionic model [30,31] was chosen. To present the possible constituents it may be expressed as: $(Ba^{2+},Ce^{3+},Cs^{+},Gd^{3+},La^{3+},Mo^{4+}, Pd^{2+},Pu^{3+},Ru^{4+},U^{4+}, Zr^{4+})_P(I^{-}, MoO_4^{2-}, O^{2-}, Va^{Q-}, CeO_2, CsO_2, Cs_2Te, I_2, MoO_3, O, Te, PuO_2, TeO_2)_Q$.

The TAF-ID describes the main metallic phase (also called "white phase") encountered in examinations of spent fuel [32] as an HCP structure with two sublattices: (Ba, Ce, Cs, Gd, Mo, Pd, Pu, Ru, U, Zr)$_1$(O, Va)$_{0.5}$.

One of the main oxide phases encountered is the perovskite structured $BaZrO_3$ [32]. This phase is sometimes referred to as the "gray phase", and in the TAF-ID it is expressed (within the CEF) as: $(Ba^{2+})_1 (Ba^{2+},U^{4+},U^{6+},Zr^{4+})_1 (O^{2-})_3$. Other fission product phases such as CsI, Cs_2Te, Cs_2MoO_4, and $BaMoO_4$ are treated as stoichiometric compounds, which means that their compositions are fixed and their Gibbs energy functions depend only on temperature and pressure. Up to now, the TAF-ID can be directly used with Thermo-Calc [33] or OpenCalphad codes and a thermodynamic database converter has recently been developed in order to be able to use it with FactSage (in ChemSage format). Parts of the TAF-ID was converted to this format for use in the Thermochimica-Bison coupling mentioned in the introduction [34].

TBASE [35,36], on its side, is a thermodynamic database elaborated at ECN Petten (Netherlands) in the 1990's which contains mainly stoichiometric compounds from reference [37]. This is the case for most solid phases, and all liquid phases. The two notable exceptions concern the fluorite fuel phase and the metallic "white phase". The thermodynamic description of the fuel phase is represented by the variable stoichiometry species model of Lindemer & Besmann [38–40]. It can be written as a solution between the following constituents: UO_2, $U_2O_{4.5}$, U_3O_7, MoO_2, MoO_3, Cs_2O, Cs_2O_2, CsO_2, $Gd_{4/3}O_2$, UGd_2O_6, $La_{4/3}O_2$, ZrO_2, $BaUO_4$, BaO, $U_{1/3}$, $U_{1/3}Pu_{4/3}O_2$, CeO_2, $Ce_{4/3}O_2$, $Pu_{4/3}O_2$, and PuO_2. The metallic phase is defined as an ideal solution between Mo, Ru, and Pd. It can be noted that in all definitions above, only the elements used in this work has been included in the expression of the phases. Moreover, the TAF-ID, unlike the TBASE description, includes heat capacity data for most phases. While heat capacity data is not required to perform the calculations presented in this work, a future improvement of the Germinal V2 code could be to couple the results of the thermodynamic model to the heat transfer model. If this were to be done, the heat capacity data for the involved phases would be necessary.

3.2 Computation times

A complete fuel pin simulation with Germinal V2 can require millions of equilibrium calculations, implying a huge computational cost associated to the thermodynamic software.

A number of test equilibrium calculations were performed by OpenCalphad and Ange over a temperature range of 500–2500 K, with a composition corresponding to a $(U_{0.78},Pu_{0.22})O_{1.975}$ fuel pin irradiated to 13.4 %FIMA burnup. Here, in order to facilitate the performance evaluation, both solvers were used in their stand-alone mode, i.e., not coupled to Germinal V2. The composition was taken from previous calculations performed by the Eranso code [41] using nuclear data from the JEFF-3.1 [42] project library. As can be seen in Table 2, 15 element groups representative of the FP, the actinides, and the oxygen were considered in the equilibria.

3.3 Germinal V2 fuel performance code

The Germinal V2 fuel performance code is being developed by the CEA, and works under the Pleiades simulation platform [7]. The code implements a 1½-D approach for the discretization of the fuel pin geometry. This means that the pin is divided into axial cells, and each axial cell is then divided into radial cells by assuming cylindrical symmetry. Here, one radial cell may represent either the fuel itself, the gap, or the cladding. One simulation is then divided into different timesteps.

In reality, the relevant physical phenomena, e.g. swelling, temperature distribution, cracking, actinide and oxygen redistribution etc. are all coupled to one another. In order to describe all these phenomena, Germinal V2 uses a scheme of nested convergence loops. In practice this means that one timestep consists of one loop over the axial cells, and within the evaluation of each axial cell another convergence loop solves the necessary equations within each radial cell. The modeling of the thermal and mechanical behavior is treated by the finite element

Table 2. Composition of equilibrium calculation used to evaluate time requirements of the different codes. The composition corresponds to $(U_{0.78},Pu_{0.22})O_{1.975}$ fuel pin irradiated to a burnup of 13.4 %FIMA.

Element	Amount [mole]
Ba (+Sr)	1.6870×10^{-2}
Ce (+Pr)	2.0673×10^{-2}
Cs (+Rb)	2.4239×10^{-2}
Gd (+Nd +Pm + Sm +Eu)	3.0816×10^{-2}
He (+Kr +Xe)	3.4776×10^{-2}
I (+Br)	2.3253×10^{-3}
La (+Y)	1.0105×10^{-2}
Mo	2.9302×10^{-2}
O	1.9750
Pd (+Ag +Cd + In +Sn +Sb)	2.5383×10^{-2}
Pu (+Am +Cm +Np)	1.8737×10^{-1}
Ru (+Tc +Rh)	4.1675×10^{-2}
Te (+Se)	5.3815×10^{-3}
U	6.7757×10^{-1}
Zr (+Nb)	2.7160×10^{-2}

solver Castem2000 [43]. The description of clad mechanical behavior (irradiation and thermal-activated creep, irradiation-induced swelling, plasticity in transient conditions) allows to account for clad deformation when evaluating the fuel-to-clad gap width. The chemical composition at each radial node of the fuel is obtained from a simplified neutronic module implementing an isolated resolution of the Bateman equations.

The coupling of Germinal V2 with a thermodynamic software (Ange or OpenCalphad) elaborated in the frame of this work allows the thermodynamic equilibrium calculation at each node of the fuel pellet, and based on the amount of gas and liquid that is found, along with the fission gas release fraction, a corresponding amount is released into the fuel-to-clad gap. The volatile release fraction is taken to be equal to that of the inert fission gases, which is an assumption with some experimental justification [44]. The model used to calculate the fission gas release is described in reference [6].

This kind of thermodynamic calculation is used to find the equilibrium state of the chemical system defined by its composition, temperature, and pressure. It does not give information regarding the kinetics of the chemical reactions. For the calculations performed inside the fuel performance code in this work, the equilibrium state is assumed to occur instantaneously due to the high temperature.

Currently, the fuel equilibrium calculations involve 15 representative elements listed in Table 2, where the elements that have been regarded as identical to its representative element are shown in the parenthesis. For example, Ba (+Sr) means that the molar amount of Sr has been added to the amount of its representative element Ba.

- Ba and Sr were grouped together since they are both believed to be (mainly) found in the $Ba(Zr,U)O_3$ and $Sr(Zr,U)O_3$ [45,46]. Their binary phase diagram shows a large degree of mutual solubility [47].
- Ce and Pr are both expected to be found in solution with the fuel matrix [45].
- Cs and Rb are both alkali metals and are expected to behave similarly [45].
- Gd, Nd, Pm, Sm, and Eu are all rare earth metals and are expected to be found in solution with the fuel matrix [32,45].
- He, Kr, and Xe are noble gases and do not react chemically with the fuel [32].
- I and Br are both halogens, easily volatilized, and grouped together in Ref. [45]. Br itself is not described by the TAF-ID.
- La and Y are believed to stay in the fuel matrix, both with valency +3 [45].
- Pd, Ag, Cd, In, Sn, and Sb are all chemically represented by Pd. They have been found in solution with each other [32]. These elements are expected to form metallic precipitates.
- Pu, Am, Cm, and Np are all represented by Pu since they are expected to stay in the fuel matrix. These elements form fluorite structure dioxides, all with similar lattice parameters [48].
- Ru, Rh, and Tc are all expected to form metallic precipitates together with the Pd-group and Mo [49]. They are grouped together and represented by Ru.
- Te and Se both belong to the chalcogen group in the periodic table, and have fairly similar chemical properties [50,51], and are represented by Te since it is the more abundant and well studied element of the two [32].
- Zr and Nb are commonly grouped together [45]. While this has been done in this work as well, it is of little consequence due to the low fission yield of Nb.

The decision to make groups of representative elements was made due to the demand to keep computational cost, complexity, and failure rates sufficiently low while still describing a chemical system as close as possible to the real one. In addition, elements needed to be grouped when they were not described in both databases, since the comparison required that the same input was used in all cases.

Among the main parameters for fuel chemistry simulation is the radial oxygen redistribution, and in Germinal V2 it is based on the work of Aitken [52]. At each axial cell, the average O/M ratio is calculated by a correlation based on the burnup, and then, depending on the radial temperature profile, the O/M radial redistribution is calculated, fixing for each radial cell its local O/M ratio. Here O/M refers the ratio between oxygen atoms and metallic atoms in the fluorite phase. An equilibrium calculation in each radial cell will tell the code how much of each element is found in a volatile phase.

Once the amount of released FP has been calculated, the JOG thickness calculation can be summarized into the following steps:

Table 3. Data used for calculations described in Section 3.3. In all cases, the solid density has been used for both the solid and liquid phases.

Compound	ρ [g/cm^3]	Ref.
Cs_2UO_4	6.6	[57]
Cs_2Te	4.25	[58]
CsI	4.53	[59]
Cs_2MoO_4	4.38	[60]
$BaUO_3$	7.58	[61]

- Obtain the molar quantity of each phase in the gap by performing a thermodynamic calculation with the released element quantities as input data.
- Estimate the molar volume of each phase found in the gap by thermodynamic calculation based on their density (see Tab. 3) and molar mass.
- Calculate the total JOG volume by summing the volume contribution of each phase. Alternatively, in a simplified approach, the JOG volume can be approximated by omitting the thermodynamic evaluation of the gap, and assuming that all released FP will enter an imaginary phase with a molar volume equal to that of Cs_2MoO_4, as it is believed to be the main JOG component [1,53,54]. Since oxygen is not included in the transport model, one mole of volatile fission products produces one third of a mole of this Cs_2MoO_4 like imaginary phase (two moles of volatile Cs and one mole of volatile Mo makes one mole of Cs_2MoO_4). The amount of available oxygen is assumed to be sufficient to oxidize with all the released FP. From a more general point of view, choosing a Cs_2MoO_4 like phase to represent all of the JOG is practical for the simulation of heat transfer in Germinal V2 since its thermal conductivity is relatively well studied [55,56].
- Regardless of how the JOG volume is obtained, by assuming that the JOG layer is uniform in thickness within each axial slice, JOG thickness, x_{JOG}, can be calculated by the equation:

$$x_{\mathrm{JOG}} = \frac{V_{\mathrm{JOG}}}{2h\pi r_{\text{fuel-outer}}} \quad (1)$$

where V_{JOG} is the JOG volume, h is the height of the axial slice, $r_{\text{fuel-outer}}$ is the outer radius of the fuel.

The process can be summarized into the flowchart presented in Figure 2.

In the chemical simulation of the fuel, the 15 families of elements from Table 2 are considered for both softwares, and in the computational model, the following FP were considered volatile and thus to be potential components of the JOG: barium, caesium, iodine, molybdenum, palladium, and tellurium. In addition to the volatile fission products, the thermodynamic evaluation of the gap included uranium, plutonium, and oxygen. Here, uranium and plutonium were added to allow the gap components to react with the outer wall of fuel.

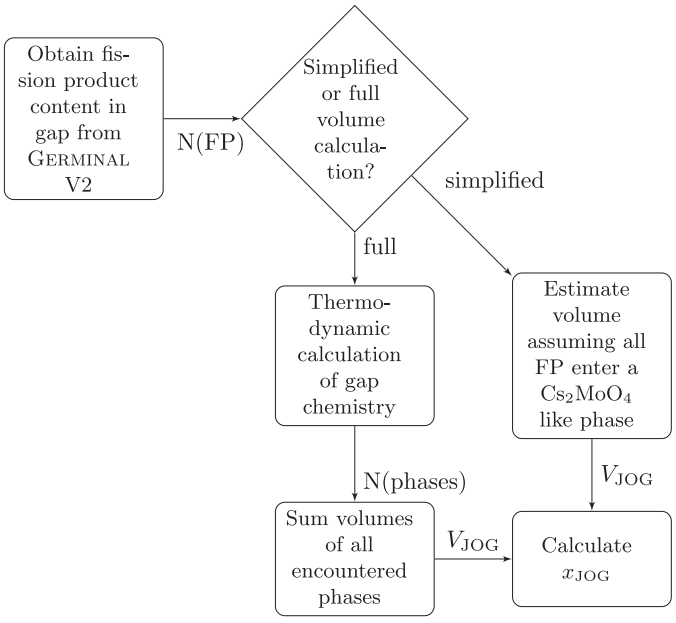

Fig. 2. Flowchart presenting the scheme for calculating the JOG width based on the predicted elements found in the gap.

Molybdenum and caesium were included since Cs_2MoO_4 is commonly believed to be the main JOG component [1], while barium, tellurium, palladium, and iodine may vaporize at the relevant fuel temperatures and are considered as volatile fission products [3]. In the PIE of one of the fuel pins mentioned in Section 2, all the considered elements had elevated concentrations in the fuel-to-clad gap.

At room temperature, where the JOG width measurements were performed, there is no stable liquid phase. This is not the case for the in-pile conditions, where temperature can reach around 1000 K in the gap. Thus, when calculating the JOG thickness using the method above, there may be liquid phases present. Whether or not these liquids contribute to the JOG thickness is unclear, since it is not known to what extent they migrate axially. In any case, it is not expected to occur at the same rate as the radial migration since the temperature gradient is at least three orders of magnitude smaller. Available oxygen in the gap is another factor which complicates the JOG width calculations. While it is obvious that oxygen should be included in the thermodynamic evaluation of the gap, the true amount is not known. In this work, $(U_{0.8},Pu_{0.2})O_{2\pm x}$ was added to the equilibrium to allow the gap components to react with the fuel. Using this method, it was possible to adjust the oxygen content so that the impact of oxygen potential could be explored. This analysis was only done on the fuel pin with highest burnup, and was carried out by including slightly hypo- and hyper-stoichiometric fuel to the JOG composition. The oxygen redistribution that occurs due to the thermal gradient tends to keep the peripheral O/M ratio close to 2, both before and after the increasing burnup causes the *global* O/M ratio to reach or even surpass 2 [5,62]. The purpose of these calculations was to investigate how the JOG composition changes at

Table 4. Computation times for the different software and configurations. Here, the 13.4 %FIMA fuel pin chemistry was used as input. 2000 calculations were performed for each configuration, between 500 K and 2500 K. Total duration corresponds to the time required for all 2000 calculations, mean and median durations are self-explanatory.

Duration [s]	Ange+TBASE	OC+TBASE	OC+TAF-ID	OC+TAF-ID
-Total	23.133	10.460	4663.318	150.615
-Mean	0.012	0.005	2.332	0.075
-Median	N/A	0.005	2.180	0.052
Comment	Ange does not use a global minimizer	Only using global minimizer when needed	Always using global minimizer	Using a library of save-files

very high burnup when assuming the local O/M ratio at the periphery can surpass 2.

Another factor that complicates the thermodynamic simulation of the JOG is the impact of the cladding elements. This has not been considered in the current work, but the treatment of the ROG ("Réaction Oxyde-Gaine" in French, also known as FCCI = Fuel Cladding Chemical Interaction) is planned to be included in future improvements of the Germinal V2 code.

Lastly, the method presented above assumes a smooth uniform layer of JOG in order to calculate the thickness while actual observations reveal a rough, porous structure. This point should be kept in mind when evaluating the results in this work since the porosity may increase the effective JOG volume considerably.

4 Results

4.1 Computation times

The test calculations, using the final (global) composition of the 13.4 %FIMA fuel pin, for obtaining the computational time for the different softwares are presented in Table 4. Results from these calculations can also be found in Figure 3, where the amount of gaseous and liquid phases are shown at different temperatures. Initially OC suffered from a considerable slow-down due to the complexity of the equilibria, but the implementation of an improved solving algorithm improved computation times. Further improvements were obtained by creating a database of solved equilibria, and using these as initial guesses for the calculations (see Sect. 5.1 for more details).

4.2 Release into gap

The maximum amount of released FP allowed by the model is the extreme case where all liquid and gaseous phases are transported into the fuel-to-clad gap. This case is illustrated in Figure 4 for the different fuel pins and softwares. Here, the distributions between the volatile fission products are presented, as well as the ratio between OC and Ange regarding released amount of FP into the gap at the peak power node.

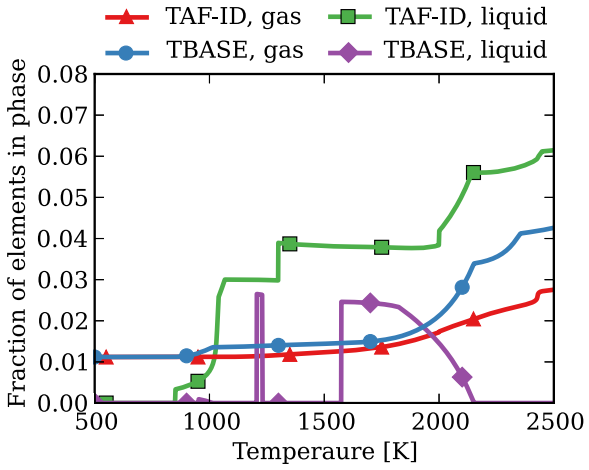

Fig. 3. Results from the test calculations of the 13.4 %FIMA fuel pin, mentioned in Section 3.2. For TAF-ID, OC has been used, and for TBASE, Ange. It can be noticed that OC+TAF-ID predicts a higher fraction of liquid phases.

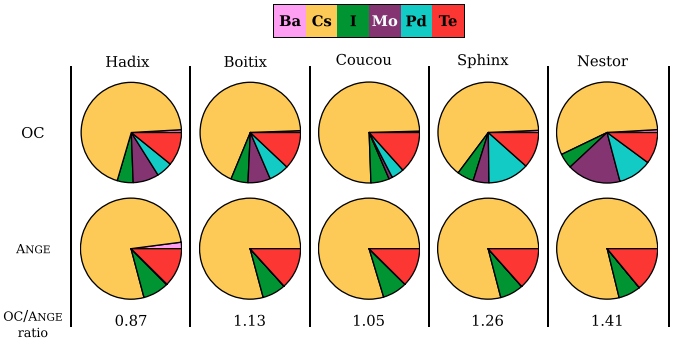

Fig. 4. Distribution of predicted released fission products in the different irradiation experiments described in Table 1. The bottom row is the ratio between the total released amount predicted by OC and Ange. All data is taken from the maximum power node.

4.3 JOG thickness vs burnup

The predicted JOG widths for the different fuel pins are presented in Figure 5. Here, the results are divided into three different subplots. The first is showing the results when the simplified mean molar volume method has been used. The second and third subplots correspond to gap

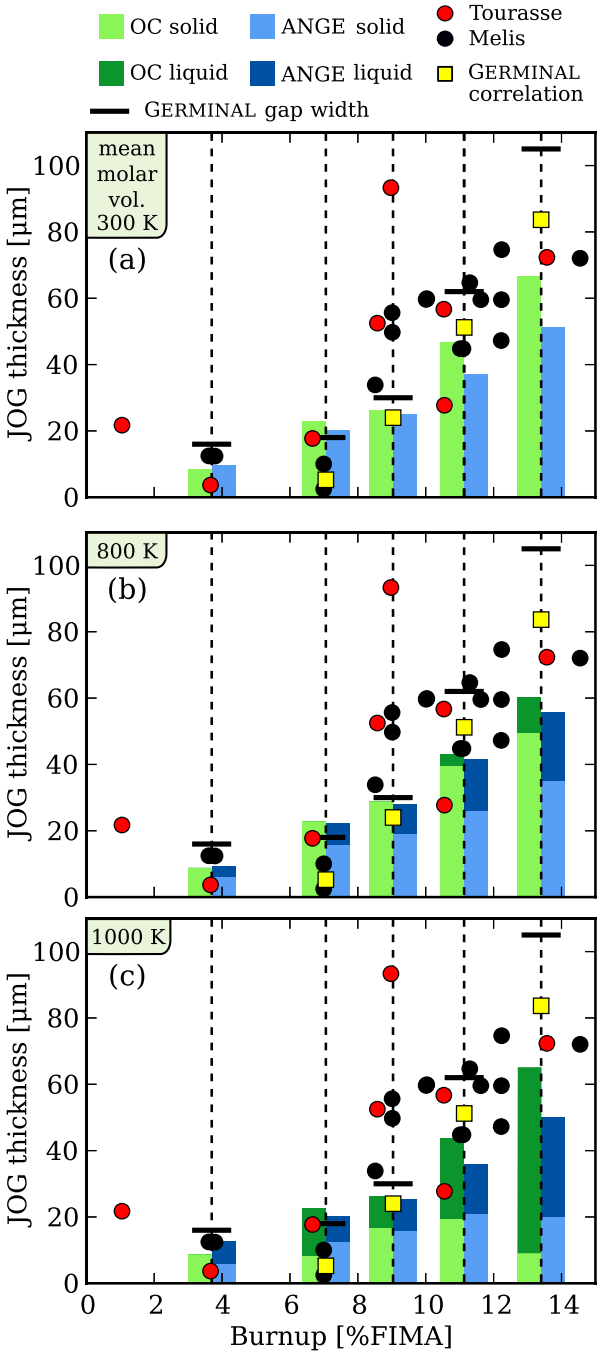

Fig. 5. JOG thickness predicted by ANGE and OC. In (a), a uniform molar volume corresponding to that of Cs_2MoO_4 at room temperature has been assumed for all fission products. In (b) and (c) the gap composition has been evaluated thermodynamically at 800 K (b), and 1000 K (c). In Tourasse (red dots) [1], the burnup values refer to the local burnup at which the JOG was measured. In Melis (black dots) [8], the burnup refers to the maximum burnup reached in the fuel pin.

compositions that have been thermodynamically evaluated at 800 K and 1000 K, respectively. Here, in order to make the calculations of the fuel pins directly comparable to one another, the oxygen content was chosen to correspond to fluorite O/M ratio as close as possible to 2. The value was chosen based on results from the GERMINAL V2 calculations, and is representative of the increase of this ratio with increasing burnup. Included also in this figure is the predicted JOG thickness calculated by the previous, correlation-based model used by GERMINAL V2. Since both solvers predicted both solid and liquid phases in the gap, the results were divided into solid and liquid thickness. The gap width predicted by GERMINAL V2, defined by the distance between the outer fuel surface and the inner clad surface, has also been included.

4.4 Thermodynamic calculation of the JOG composition

In order to see how the oxygen potential affects the chemical state in the gap, calculations on the final gap composition of the 13.4 %FIMA irradiated fuel pin were performed together with $(U_{0.8},Pu_{0.2})O_{2\pm x}$ (where x is the deviation from stoichiometry and depends on the oxygen potential). In Figure 6, the results from calculations just above and just below O/M = 2 are presented.

5 Discussion

5.1 Computation times

Figure 3 shows the predicted fraction of elements in a volatile state (here meaning both gaseous and liquid) in the test calculations using the input of Table 2. The TAF-ID calculations predict a higher tendency towards volatilization. Looking at the difference in the amount of liquid, the behavior becomes more pronounced. This is a consequence of the different models used for describing the liquid phases. As mentioned in Section 3.1, the TAF-ID uses the more advanced ionic liquid model based on the CEF, while the only liquid phases allowed in the TBASE calculations are the molten stoichiometric phases. This difference in models stabilizes the liquid phases (both against solid and gaseous phases) for the TAF-ID calculations. The TBASE calculations do not predict any melting of the precipitated metallic phase (Pd,Mo,Ru), while the TAF-ID calculations predict onset and completion of the melting of the metallic phases at around 1000 K and 2200 K, respectively. The increased complexity of the TAF-ID causes a noticeable increase in computation time compared to TBASE, which is an obvious drawback. In the case of a nuclear fuel simulation, however, most equilibria do not differ significantly from one another in terms of composition and temperature. This circumstance allows for considerable speedup when using OPENCALPHAD, because a large fraction of the computation time is normally spent finding a reasonable initial guess, using a grid minimizer described in references [21,22] based on the approach of Chen et al. [63,64]. If most calculations are similar in temperature and composition, a previous equilibrium can be used as an initial guess. In this work a method that saves and reads equilibria for initial guesses has been implemented, significantly improving computation times. Naturally, generating the initial library of necessary saved equilibria will still cost computational

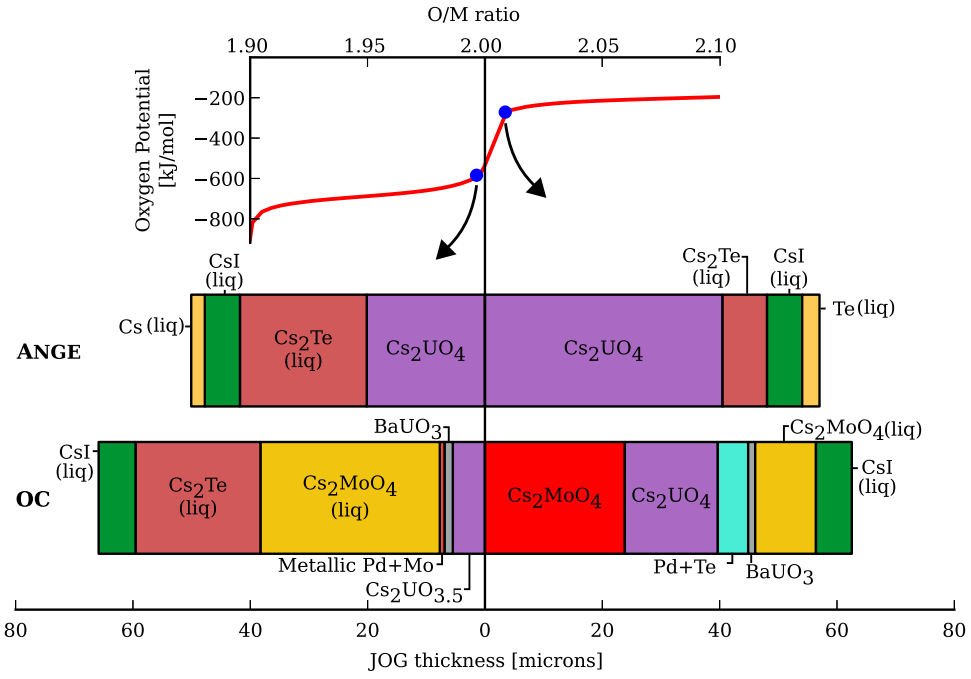

Fig. 6. JOG widths for the 13.4 %FIMA fuel pin calculated by OC and Ange at 1000 K. The left case is just before the oxidation of Mo is complete, and the fluorite O/M ratio is just below 2. In the right case, oxygen amount has been slightly increased so that all Mo is oxidized, and the O/M ratio is just above 2.

time. Another aspect of OpenCalphad which has been explored, but not yet implemented into Germinal V2, is the ability to solve several equilibria in parallel, which would obviously open the possibility for further improvements.

5.2 Release into gap

The results in Figure 4 show that the OC+TAF-ID configuration predicts a larger amount of released FP in all cases except for the fuel pin with the lowest burnup. A similar trend can be seen in Figure 3, which shows the amount of predicted gas and liquid in the test calculations discussed in Section 3.2. This difference can be explained by the fact that Ange+TBASE predicts almost no liquid Ba and Mo compared to OC+TAF-ID.

5.3 JOG thickness versus burnup evaluation

The results from the Germinal V2 calculations and subsequent thermodynamic evaluation of the chemical composition of the gap show that the method used allows the prediction of JOG widths at least comparable to the measured values. For the two fuel pins with lowest burnup, the calculations generally overpredict the widths. In the 7 %FIMA case, the predicted JOG widths even slightly (less than 5 µm) exceed the predicted fuel-clad gap width. This can probably be explained by the fact that the model (incorrectly) assumes instantaneous transport of the FP into the gap. This could be corrected by introducing a threshold burnup at which the JOG is expected to appear (as is the case for the Germinal V2 correlation based model).

The comparison between the results from the thermodynamic models presented in this work and the JOG widths predicted by the correlation based model in Germinal V2 shows a better agreement. The largest discrepancy between these models is seen in the fuel pin with highest burnup, where the thermodynamic calculation method underpredicts the JOG thickness compared to both the measurement and correlation model. In the 9.0 %FIMA fuel pin (Coucou-1), neither model was able to predict the jump in JOG width seen by the PIE. This could be explained by considering its comparatively low irradiation temperature. A lower temperature corresponds to a smaller fraction of volatile phases as well as a weaker propensity for radial migration due to the lower temperature gradient.

For the two fuel pins with highest burnup, the models slightly underpredict the JOG widths. One possible explanation here is that the measured gap was not entirely a consequence of the presence of FP compounds. As mentioned in Section 2, the experiments do not differentiate between the JOG and the gas gap when measuring the JOG width. The thickness of the JOG is assumed to be equal to the measured width since the gap is expected to be closed due to swelling at this point.

What can be noted regarding the results is the rather high amount of liquid phases in all calculations of the 1000 K case. When the temperature was decreased to 800 K, the amount of liquid decreased, and in some cases vanished completely. If the liquid phases are included in the JOG width calculations, there is no significant difference between the thermodynamic evaluation method and the mean molar volume method. While the simplified

method appears adequate at predicting the JOG thickness, it can not be used when studying the consequences of the fission product layer, such as the change in thermal conductivity, and potential chemical interaction with the cladding. This is due to the fact that the simplified model does not give any information regarding the actual chemistry in the gap: everything is assumed to be an imaginary Cs_2MoO_4 like phase.

In all cases, as can be seen, in Figure 4, Cs is the major contributor to the FP in the gap. In the Ange calculations, only Cs, Te, and I were released (as well as low amounts of Ba). The OC calculations, using the more advanced database which allows ionic liquids, predicted the release of Mo and Pd in addition to those in the Ange calculations. The TBASE database utilized by Ange lacks a thermodynamic description of the liquid metallic Mo and Pd phases. For volatilization to occur, evaporation is required.

The varying fraction of released Mo in the OC calculations can be explained by the maximum temperatures during irradiation of the different fuel pins. Mo is only released when the temperature is above ∼2000 K, so in order to get a relatively high Mo content in the gap, there needs to be either high operating conditions all along the irradiation or at least one period of high temperature at the end of irradiation (when the total Mo inventory has accumulated). This is not the case in Coucou-1 (and Sphinx-1 to a lesser extent) irradiation experiments, and thus the Mo release is lower here.

When performing gap calculations, the most common solid phases were $Cs_2UO_{3.5-4}$. The metallic phase contained mostly Pd and Te, with low fractions of Mo. The most common liquid phases were Cs_2Te, Cs_2MoO_4 and CsI.

5.4 Thermodynamic calculation of the JOG composition

In the case of the highest burnup fuel pin, an examination of the impact of oxygen potential, which is known to increase with burnup, was performed. Calculations on the gap compositions together with $(U_{0.8},Pu_{0.2})O_{2\pm x}$ were performed in order to see what happens to the predicted phases as the O/M ratio shifts from below to above the critical value of 2. In the Ange case, as can be seen in Figure 6, the added oxygen causes the amount of Cs_2UO_4 to increase, while absorbing some of the caesium of the Cs_2Te phase. In the OC case where a significant amount of molybdenum is present (unlike the Ange case), a partial solidification of the Cs_2MoO_4 phase is seen. The molybdenum which is in the metallic form at lower oxygen potential oxidizes, as expected. All of the caesium from the Cs_2Te is absorbed into the Cs_2MoO_4 and Cs_2UO_4 phases. The tellurium, together with the metallic palladium, form the intermetallics Pd_8Te_3 and $PdTe_2$. In both the OC and Ange cases, the liquid CsI remains unchanged by the rise in oxygen potential.

The presence of Cs_2MoO_4 in the calculations discussed here and in Section 5.3 justifies, at least to some extent, the assumptions of the mean molar volume method presented in Section 3.3.

Different options regarding the treatment of the gap chemistry have been explored in this work. There are still several variables that affect the outcome of the thermodynamic calculations in the gap, mainly which elements to include and their respective quantities. Including or discarding fuel and cladding elements in the equilibrium calculations directly or indirectly determines what chemical phases are stable in the gap. In reality, it may also be the case that the inner part of the JOG layer contains fuel elements, while the outer part contains cladding elements. Indeed, small quantities of uranium as well as cladding material was found inside the JOG in the PIE of one of the studied fuel pins. If this is the case, the fuel-to-JOG and JOG-to-clad borders become blurred, and the JOG thickness becomes more complicated to properly define. This can be seen in thermodynamic evaluation of the fuel composition performed in this work. The caesium, together with uranium, forms the oxide phases $Cs_2UO_{3.5-4}$, when there is not enough molybdenum to form Cs_2MoO_4.

6 Outlook

The volatile fission product release fraction has been approximated to correspond to that of stable fission gases, based on the correlation used by Germinal V2. A future improvement could be to couple the JOG prediction model with the Margaret [65] fission gas transport code in order to describe more accurately the volatile fission product release rate. Indeed, new functionalities have been added to the current version of the code, designated Margaret PAF, in order to describe the creation, destruction (by decay or by neutronic reaction), and transport of isotopes in the grain and along the grain boundaries.

One factor which has not been accounted for in this work is the JOG porosity. The theoretical density has been used in both of the methods for calculating the JOG thickness, which is expected to underpredict the thickness. Future experiments could help improve the understanding of the JOG microstructure, and thus provide a value for the porosity that could be used in the model. It may, however, be speculated that any measurements would yield a range of values for the porosity, due to the known heterogeneity in composition in the JOG. More detailed PIE focusing on the JOG could illuminate which phases are present in the gap, and the ratios between the present volatile FP. This could also help to clarify whether or not the high fraction of liquid phases in the gap, which is encountered in some of the calculations, is possible. This information could then be implemented to improve the approach presented in this work.

7 Conclusions

By coupling thermodynamic calculations to the Germinal V2 fuel performance code, a method for calculating the JOG width has been developed. Additionally, the approach is able to illuminate the question of which

elements and phases are likely to be encountered in the JOG.

In the Ange+TBASE setup, neither molybdenum nor palladium was found released into the fuel-to-clad gap. Based on PIEs, both of these elements are expected to migrate towards the periphery and into the gap. Thus, the added computational cost of using OC+TAFID over Ange+TBASE becomes justified by the improvement in predicted fuel chemistries.

In this work, only Ba, Cs, I, Mo, Pd, O Te, U, and Pu have been included in the gap calculations. While it is not obvious how to choose the oxygen content in the gap, different approaches have been tested in this work.

The implementation of thermodynamic calculations into a fuel performance code allows for the possibility of coupling several additional models. For example, the modeling of heat transfer, oxygen and actinide redistribution (by solid or gaseous diffusion), axial redistribution of JOG components, and internal cladding corrosion could all benefit from the calculations performed by the thermodynamic software. This last aspect is planned to be implemented in the future.

The authors would like to acknowledge the funding received from the Euratom research and training programs 2014–2018 under the Grant Agreements No. 754329 (INSPYRE) and 2013-08859 (SAFARI). This work contributes to the Joint Programme of Nuclear Materials (JPNM) of the European Energy Research Alliance (EERA). The authors would also like to thank Romain Le Tellier and Clément Introïni for their help with the integration of OpenCalphad into Germinal V2, as well as Christine Guéneau for her support with the TAF-ID.

Author contribution statement

Karl Samuelsson: Conceived of and developed the calculation model and its coupling to the fuel performance code. Performed all calculations and visualizations of results. Wrote the manuscript draft. Jean-Christophe Dumas: Conceived of and developed the model, supervised and organized the work. Bo Sundman: Developed the thermodynamic software and supervised the work. Marc Lainet: Worked on the fuel performance code, and its coupling to the thermodynamic software. All authors analyzed and discussed the results, and contributed to the final manuscript.

References

1. M. Tourasse, M. Boidron, B. Pasquet, Fission product behaviour in phenix fuel pins at high burnup, J. Nucl. Mater. **188**, 49 (1992)
2. M. Inoue, K. Maeda, K. Katsuyama, K. Tanaka, K. Mondo, M. Hisada, Fuel-to-cladding gap evolution and its impact on thermal performance of high burnup fast reactor type uranium-plutonium oxide fuel pins, J. Nucl. Mater. **326**, 59 (2004)
3. K. Maeda, 3.16 - ceramic fuel-cladding interaction, Compr. Nucl. Mater. **3**, 443 (2012)
4. International Atomic Energy Agency, Structural Materials for Liquid Metal Cooled Fast Reactor Fuel Assemblies-Operational Behaviour, number NF-T-4.3 in Nuclear Energy Series, Vienna, 2012; https://www.iaea.org/publications/8872/structural-materials-for-liquid-metal-cooled-fast-reactor-fuel-assemblies-operational-behaviour
5. Y. Guerin, Fuel performance of fast spectrum oxide fuel, in *Comprehensive Nuclear Materials*, edited by R.J. Konings (Elsevier, Oxford 2012), pp. 547–578
6. M. Lainet, B. Michel, J.-C. Dumas, M. Pelletier, I. Ramière, Germinal, a fuel performance code of the pleiades platform to simulate the in-pile behaviour of mixed oxide fuel pins for sodium-cooled fast reactors, J. Nucl. Mater. **516**, 30 (2019)
7. V. Marelle, Validation of PLEIADES/ALCYONE 2.0 fuel performance code, *Water Reactor Fuel Performance Meeting, Jeju, South Korea, 2017*
8. J.-C. Melis, J.-P. Piron, L. Roche, Fuel modeling at high burn-up: recent development of the germinal code, J. Nucl. Mater. **204**, 188 (1993)
9. B. Baurens, J. Sercombe, C. Riglet-Martial, L. Desgranges, L. Trotignon, P. Maugis, 3D thermo-chemical-mechanical simulation of power ramps with alcyone fuel code, J. Nucl. Mater. **452**, 578 (2014)
10. P. Konarski, J. Sercombe, C. Riglet-Martial, L. Noirot, I. Zacharie-Aubrun, K. Hanifi, M. Frégonèse, P. Chantrenne, 3d simulation of a power ramp including fuel thermochemistry and oxygen thermodiffusion, J. Nucl. Mater. **519**, 104 (2019)
11. S. Simunovic, J. W. Mcmurray, T. M. Besmann, E. Moore, M.H.A. Piro, Coupled Mass and Heat Transport Models for Nuclear Fuels using Thermodynamic Calculations, Technical Report, Oak Ridge National Laboratory, 2018
12. M. Piro, S. Simunovic, T. Besmann, B. Lewis, W. Thompson, The thermochemistry library thermochimica, Comput. Mater. Sci. **67**, 266 (2013)
13. R. Williamson, J. Hales, S. Novascone, M. Tonks, D. Gaston, C. Permann, D. Andrs, R. Martineau, Multidimensional multiphysics simulation of nuclear fuel behavior, J. Nucl. Mater. **423**, 149 (2012)
14. T. Uwaba, J. Nemoto, I. Ishitani, M. Ito, Coupled computer code study on irradiation performance of a fast reactor mixed oxide fuel element with an emphasis on the fission product cesium behavior, Nucl. Eng. Des. **331**, 186 (2018)
15. M. Ishida, et al., in *Proceedings of the fall meeting of the atomic energy society of Japan, 1987*, p. J77
16. Y. Saito, et al., in *Proceedings of the fall meeting of the atomic energy society of Japan, 1988*, p. H14
17. T. Uwaba, T. Mizuno, J. Nemoto, I. Ishitani, M. Ito, Development of a mixed oxide fuel pin performance analysis code "CEDAR": Models and analyses of fuel pin irradiation behavior, Nucl. Eng. Des. **280**, 27 (2014)
18. P. Spencer, A brief history of CALPHAD, Calphad **32**, 1 (2008)
19. U.R. Kattner, The Calphad method and its role in material and process development. Tecnol. Metal. Mater. Min. **13**, 3 (2016)
20. P. Garcia, J.P. Piron, D. Baron, A model for the oxygen potential of oxide fuels at high burnup, Technical Report, International Atomic Energy Agency (IAEA), 1997, http://inis.iaea.org/search/search.aspx?orig_q=RN:28068403

21. B. Sundman, U.R. Kattner, M. Palumbo, S.G. Fries, Opencalphad – a free thermodynamic software, Integr. Mater. Manuf. Innov. **4**, 1 (2015)
22. B. Sundman, X.-G. Lu, H. Ohtani, The implementation of an algorithm to calculate thermodynamic equilibria for multi-component systems with non-ideal phases in a free software, Comput. Mater. Sci. **101**, 127 (2015)
23. T. Besmann, *SOLGASMIX-PV, a computer program to calculate equilibrium relationships in complex chemical systems* (Oak Ridge National Lab., TN, USA, 1977)
24. G. Eriksson, Thermodynamic studies of high temperature equilibria. XII. SOLGASMIX, a computer program for calculation of equilibrium composition in multiphase systems, Chem. Scr. **8**, 100 (1975)
25. C. Weber, Convergence of the equilibrium code solgasmix, J. Comput. Phys. **145**, 655 (1998)
26. TAF-ID homepage, 2019, https://www.oecd-nea.org/science/taf-id
27. C. Guéneau, S. Gossé, A. Quaini, N. Dupin, B. Sundman, M. Kurata, T. Besmann, P. Turchi, J. Dumas, E. Corcoran, M. Piro, T. Ogata, R. Hania, B. Lee, R. Kennedy, S. Massara, FUELBASE, TAF-ID databases and OC software: Advanced computational tools to perform thermodynamic calcu-lations on nuclear fuel materials, in *Proceedings of the 7th European Review Meeting on Severe Accident Research 2015, Marseille, France, 2015*
28. M. Hillert, The compound energy formalism, J. Alloys Compd. **320**, 161 (2001)
29. C. Guéneau, N. Dupin, B. Sundman, C. Martial, J.-C. Dumas, S. Gossé, S. Chatain, F. D. Bruycker, D. Manara, R.J. Konings, Thermodynamic modelling of advanced oxide and carbide nuclear fuels: Description of the U-Pu-O-C systems, J. Nucl. Mater. **419**, 145 (2011)
30. M. Hillert, B. Jansson, B. Sundman, J. Ågren, A two-sublattice model for molten solutions with different tendency for ionization, Metall. Trans. A **16**, 261 (1985)
31. B. Sundman, Modification of the two-sublattice model for liquids, Calphad **15**, 109 (1991)
32. H. Kleykamp, The chemical state of the fission products in oxide fuels, J. Nucl. Mater. **131**, 221 (1985)
33. J.-O. Andersson, T. Helander, L. Höglund, P. Shi, B. Sundman, Thermo−Calc & DICTRA, computational tools for materials science, Calphad **26**, 273 (2002)
34. T. Besmann, J. McMurray, B. Gaston, S. Simunovic, M. Piro, Modeling thermochemistry of fuel and coupling to fuel performance codes, in *Proceedings of Top Fuel, Boise, ID, USA, 2016*
35. E.H.P. Cordfunke, R.J.M. Konings, Thermochemical data for reactor materials and fission products: The ECN database, J. Phase Equilib. **14**, 457 (1993)
36. R. Schram, R. Konings, W. Rijnsburger, TBASE CONSULT Manual, The Netherlands Energy Research Foundation ECN, 2002
37. E. Cordfunke, R. Konings, *Thermochemical Data for Reactor Materials and Fission Products* (North-Holland, Amsterdam, 1990)
38. T.B. Lindemer, T.M. Besmann, Chemical thermodynamic representation of $\langle UO_{2\pm x}\rangle$, J. Nucl. Mater. **130**, 473 (1985)
39. T.M. Besmann, T.B. Lindemer, Chemical thermodynamic representation of $\langle PuO_{2-x}\rangle$ and $\langle U_{1-z}Pu_zO_w\rangle$, J. Nucl. Mater. **130**, 489 (1985)
40. T.B. Lindemer, J. Brynestad, Review and chemical thermodynamic representation of $\langle U_{1-z}\ Ce_zO_{2\pm x}\rangle$ and $\langle U_{1-z}\ Ln_zO_{2\pm x}\rangle$; Ln = Y,La,Nd,Gd, J. Am. Ceram. Soc. **69**, 867 (1986)
41. G. Rimpault, The ERANOS code and data system for fast reactor neutronic analyses, in *Proceedings of the PHYSOR2002 International Conference on the New Frontiers of Nuclear Technology: Reactor Physics, Safety and High Performance Computing, Seoul, South Korea, 2002*
42. A. Koning, R. Forrest, M. Kellett, R. Mills, H. Henriksson, Y. Rugama, JEFF Report 21: The JEFF-3.1 Nuclear Data Library, 2006
43. P. Verpeaux, T. Charras, A. Millard, CASTEM 2000: une approche moderne du calcul des structures (Pluralis, 1988) p. 261
44. V. Bouineau, M. Lainet, N. Chauvin, M. Pelletier, V. Di Marcello, P. Van Uffelen, C. Walker, Assessment of SFR fuel pin performance codes under advanced fuel for minor actinide transmutation, American Nuclear Society - ANS; La Grange Park (United States), 2013
45. B. Lewis, W. Thompson, F. Iglesias, Fission Product Chemistry in Oxide Fuels, in *Comprehensive Nuclear Materials* edited by R.J. Konings (Elsevier, Oxford, 2012), pp. 515–546
46. J. Adams, M. Carboneau, National low-level waste management program radionuclide report series. Volume 2: niobium-94, 1995
47. T.B. Massalski, *Binary alloy phase diagrams*, 2nd edn. (ASM International, Materials Park, Ohio, 1990)
48. C. Guéneau, A. Chartier, L.V. Brutzel, Thermodynamic and thermophysical properties of the actinide oxides, in *Comprehensive Nuclear Materials* edited by R.J. Konings (Elsevier, Oxford, 2012), pp. 21–59
49. K. Naito, T. Tsuji, T. Matsui, A. Date, Chemical state, phases and vapor pressures of fission-produced noble metals in oxide fuel, J. Nucl. Mater. **154**, 3 (1988)
50. K. Bagnall, Selenium, tellurium and polonium, in *The Chemistry of Sulphur, Selenium, Tellurium and Polonium*, Pergamon Texts in Inorganic Chemistry edited by M. Schmidt, W. Siebert, K. Bagnall (Pergamon, Oxford, 1973), pp. 935–1008
51. J. McFarlane, J.C. LeBlanc, Fission-product tellurium and cesium telluride chemistry revisited, Technical Report, Canada, 1996, http://inis.iaea.org/search/search.aspx?orig_q=RN:29054591
52. E. Aitken, Thermal diffusion in closed oxide fuel systems, J. Nucl. Mater. **30**, 62 (1969)
53. A. Karahan, J. Buongiorno, Modeling of thermo-mechanical and irradiation behavior of mixed oxide fuel for sodium fast reactors, J. Nucl. Mater. **396**, 272 (2010)
54. J. Rouault, P. Chellapandi, B. Raj, P. Dufour, C. Latge, L. Paret, P. Pinto, G.H. Rodriguez, G.-M. Gautier, G.-L. Fiorini, M. Pelletier, D. Gosset, S. Bourganel, G. Mignot, F. Varaine, B. Valentin, P. Masoni, P. Martin, J.-C. Queval, D. Broc, N. Devictor, *Sodium Fast Reactor Design: Fuels, Neutronics, Thermal-Hydraulics, Structural Mechanics and Safety* (Springer US, Boston, MA, 2010), pp. 2321–2710
55. T. Ishii, T. Mizuno, Thermal conductivity of cesium molybdate Cs_2MoO_4, J. Nucl. Mater. **231**, 242 (1996)
56. T. Ishii, T. Mizuno, An investigation of the thermal conductivity of Cs_2MoO_4, J. Nucl. Mater. **247**, 82 (1997)
57. M. Takano, K. Minato, K. Fukuda, S. Sato, H. Ohashi, Thermal expansion and thermal conductivity of cesium uranates, J. Nucl. Sci. Technol. **35**, 485 (1998)

58. I. Schewe-Miller, P. Böttcher, Synthesis and crystal structures of K_5Se_3, Cs_5Te_3 and Cs_2Te, Z. Kristallograph. **196**, 137 (1991)
59. T.B. Rymer, P.G. Hambling, The lattice constant of caesium iodide, Acta Crystallograph. **4**, 565 (1951)
60. F.X.N.M. Kools, A.S. Koster, G.D. Rieck, The structures of potassium, rubidium and caesium molybdate and tungstate, Acta Crystallograph. Sect. B **26**, 1974 (1970)
61. A. Reis, H. Hoekstra, E. Gebert, S. Peterson, Redetermination of the crystal structure of barium uranate, J. Inorg. Nucl. Chem. **38**, 1481 (1976)
62. C. Sari, G. Schumacher, Oxygen redistribution in fast reactor oxide fuel, J. Nucl. Mater. **61**, 192 (1976)
63. C. Shuang-Lin, C. Kuo-Chih, Y. Chang, On a new strategy for phase diagram calculation 1. Basic principles, Calphad **17**, 237 (1993)
64. C. Shuang-Lin, C. Kuo-Chih, Y. Chang, On a new strategy for phase diagram calculation 2. Binary systems, Calphad **17**, 287 (1993)
65. L. Noirot, Margaret: A comprehensive code for the description of fission gas behavior, Nucl. Eng. Des. **241**, 2099 (2011)

Cite this article as: Karl Samuelsson, Jean-Christophe Dumas, Bo Sundman, Marc Lainet, An improved method to evaluate the "Joint Oxyde-Gaine" formation in (U,Pu)O_2 irradiated fuels using the GERMINAL V2 code coupled to Calphad thermodynamic computations, EPJ Nuclear Sci. Technol. **6**, 47 (2020)